frontiers in Immunology

ORIGINAL RESEARCH
published: 30 November 2021
doi: 10.3389/fimmu.2021.776933

Increased B Cell Selection Stringency In Germinal Centers Can Explain Improved COVID-19 Vaccine Efficacies With Low Dose Prime or Delayed Boost

Amar K. Garg[1†], *Soumya Mittal*[1], *Pranesh Padmanabhan*[2], *Rajat Desikan*[1†] *and Narendra M. Dixit*[1,3*]

[1] Department of Chemical Engineering, Indian Institute of Science, Bangalore, India, [2] Clem Jones Centre for Ageing Dementia Research, Queensland Brain Institute, The University of Queensland, Brisbane, QLD, Australia, [3] Centre for Biosystems Science and Engineering, Indian Institute of Science, Bangalore, India

OPEN ACCESS

Edited by:
Evelien M. Bunnik,
The University of Texas Health Science Center at San Antonio, United States

Reviewed by:
Darrell Irvine,
Massachusetts Institute of Technology, United States
Philippe Auguste Robert,
University of Oslo, Norway

***Correspondence:**
Narendra M. Dixit
narendra@iisc.ac.in

†Present address:
Amar K. Garg,
Systems Immunology Department, Helmholtz Centre for Infection Research, Braunschweig, Germany;
Rajat Desikan,
Certara Quantitative Systems Pharmacology (QSP), Certara UK Limited, Sheffield, United Kingdom

Specialty section:
This article was submitted to Systems Immunology, a section of the journal Frontiers in Immunology

Received: 14 September 2021
Accepted: 10 November 2021
Published: 30 November 2021

Citation:
Garg AK, Mittal S, Padmanabhan P, Desikan R and Dixit NM (2021) Increased B Cell Selection Stringency In Germinal Centers Can Explain Improved COVID-19 Vaccine Efficacies With Low Dose Prime or Delayed Boost. Front. Immunol. 12:776933. doi: 10.3389/fimmu.2021.776933

The efficacy of COVID-19 vaccines appears to depend in complex ways on the vaccine dosage and the interval between the prime and boost doses. Unexpectedly, lower dose prime and longer prime-boost intervals have yielded higher efficacies in clinical trials. To elucidate the origins of these effects, we developed a stochastic simulation model of the germinal center (GC) reaction and predicted the antibody responses elicited by different vaccination protocols. The simulations predicted that a lower dose prime could increase the selection stringency in GCs due to reduced antigen availability, resulting in the selection of GC B cells with higher affinities for the target antigen. The boost could relax this selection stringency and allow the expansion of the higher affinity GC B cells selected, improving the overall response. With a longer dosing interval, the decay in the antigen with time following the prime could further increase the selection stringency, amplifying this effect. The effect remained in our simulations even when new GCs following the boost had to be seeded by memory B cells formed following the prime. These predictions offer a plausible explanation of the observed paradoxical effects of dosage and dosing interval on vaccine efficacy. Tuning the selection stringency in the GCs using prime-boost dosages and dosing intervals as handles may help improve vaccine efficacies.

Keywords: SARS-CoV-2, vaccine efficacy, affinity maturation, prime-boost immunization, germinal center (GC)

INTRODUCTION

The COVID-19 pandemic continues to rage and warrants intensifying the ongoing global vaccination programs (1, 2). With limited vaccine supplies, it becomes critical to identify dosing protocols that would maximize vaccine efficacy (3, 4). With the Oxford-AstraZeneca vaccine, where dosing protocols were adjusted during the trials, data has become available of the effects of different dosages used for the prime and boost doses and of different intervals separating them on vaccine efficacy (5–8). A recent study has also examined the effects of increasing the interval beyond those

in the trials (9). Intriguingly, the efficacy in preventing symptomatic infection was 63.1% when a standard dose (containing 5×10^{10} virus particles) was used for both prime and boost, whereas the efficacy was substantially higher, 80.7%, when a low dose prime (containing 2.2×10^{10} virus particles) followed by the standard dose boost was administered (5). Furthermore, the efficacy increased with the interval between the prime and boost, from 55.1% at <6 weeks to 81.3% at ≥12 weeks, when standard doses were used for both (5). Inspired by these observations, studies are examining the effects of lower dosages and increased dosing intervals with other vaccines too, specifically the Pfizer-BioNTech (10–12) and Moderna (13) vaccines. An understanding of these effects would help identify optimal dosing protocols and maximize the impact of the ongoing vaccination programs. The origins of the effects remain to be elucidated.

While the role of cellular immunity is yet to be fully elucidated (14), several studies suggest that the efficacy of currently approved COVID-19 vaccines is attributable to the neutralizing antibodies they elicit (6, 11, 15–20). The higher efficacies observed above are thus argued to be due to the improved quality and quantity of the antibodies produced by the associated dosing protocols (5, 8, 9, 11, 21). For instance, higher antibody levels were observed following the boost upon increasing the dosing interval (9, 10). In some cases, antibody-dependent cellular functions too appeared to be better with the longer intervals (21). A question that arises is how the different dosing protocols elicit antibodies of different amounts and affinities for their targets.

Antibody production following vaccination (or natural infection) occurs in germinal centers (GCs) (22, 23). GCs are temporary anatomical structures assembled in lymphoid organs where B cells are locally selected based on the ability of their receptors to bind and internalize antigen presented as immune complexes on follicular dendritic cell surfaces in the GCs. [GCs can last anywhere from a few weeks to many months (23–25)]. This process, termed affinity maturation, culminates, typically in weeks, in the selection of B cells with affinities that can be several orders of magnitude higher for the target antigen than those at the start of the GC reaction (26, 27). What determines the final affinities is an important question in immunology and is yet to be resolved (28–30). Several studies have identified factors that influence affinity maturation (26, 31–37). A key factor is antigen availability within GCs–related here to the vaccine dosage and antigen half-life–elucidated first by the classic experiments of Eisen and colleagues (26): B cells compete for antigen in the GCs. Their survival depends on how much antigen they acquire, as we explain below. Thus, if antigen is scarce, the selection is stringent and leads preferentially to the survival of those B cells that have high affinity for the target antigen. This phenomenon governing the GC reaction is manifested widely, including in the effects of passive immunization following HIV infection, and can be potentially exploited by tuning antigen availability (34, 35, 38, 39).

Here, we reasoned that one way in which the effects of the different vaccination protocols could arise was from the influence the protocols had on antigen availability and hence selection stringency within GCs. Specifically, low dose prime is expected to result in low antigen availability and may lead to the selection of higher affinity B cells. The standard dose boost could then enable the expansion of these higher affinity B cells. With a larger dosing interval, affinity maturation is expected to proceed further before the boost, yielding higher affinity B cells for expansion post the boost. The decay of antigen between doses could cause a further increase in selection stringency, amplifying this effect. To test this hypothesis, we developed a detailed stochastic simulation model of the GC reaction. Such simulation models have been shown to mimic the GC reaction faithfully and have helped resolve confounding experimental observations and predict optimal vaccination protocols (34–36, 39–44).

RESULTS

Stochastic Simulation Model of the GC Reaction Post COVID-19 Vaccination

We present an overview of the model here (**Figure 1**); details are in Methods. We considered individuals who were not previously infected and were administered COVID-19 vaccines. We focused on the GC reaction in such individuals. The simulation, building on previous protocols (35, 36, 39, 40, 42), considered and modelled events within an individual GC. The GC reaction is initiated by B cells of low affinity for a target, non-mutating antigen. The target could be a portion of or the entire spike protein of SARS-CoV-2. We simulated the ensuing affinity maturation process using a discrete generation, Wright-Fisher-type, formalism (36, 39, 45). The GC is divided into a light zone and a dark zone (**Figure 1A**). The antigen is presented in the light zone and is represented as a bit-string of L amino acids. Each B cell is identified by its B cell receptor (BCR), which is also represented as a bit-string of L amino acids. The affinity of a B cell for the antigen is determined by the extent of the match between the BCR and antigen sequences, or 'match length', defined as the length of the longest common continuous substring (39, 42), defined here using ε. ε=0 if the two sequences are completely distinct, whereas ε=L if they are identical. The higher the ε, the higher is the affinity. In each generation, we let each B cell have an average of η attempts to acquire antigen. η thus serves as a surrogate of antigen availability in the GC (39). The probability with which a B cell acquires antigen in each attempt is set proportional to its affinity for the antigen (39). If a B cell fails to acquire a minimum amount of antigen, it is assumed to undergo apoptosis (31), and is eliminated. The surviving B cells then compete for help from T follicular helper (T_{fh}) cells. The probability that a B cell receives such help is set proportional to the amount of antigen it has acquired relative to that of the other B cells in the generation (39). B cells that do not succeed in receiving T_{fh} help are again assumed to undergo apoptosis (31). Among the surviving B cells, following previous studies (39), we let 5% exit the GC, become plasma cells, and produce antibodies; 5% exit and become memory B cells; and 90% migrate to the dark zone, where they

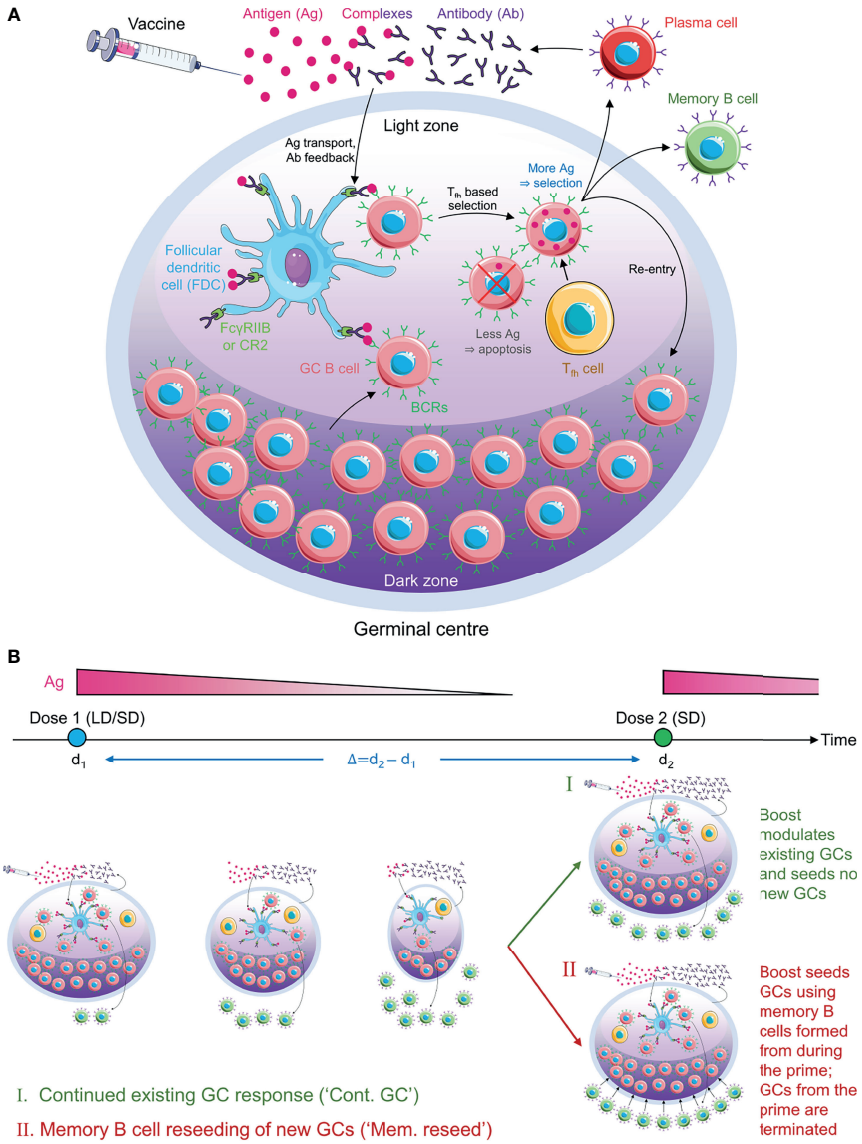

FIGURE 1 | Schematic of the GC reaction model post vaccination. **(A)** The GC reaction. The antigen from the vaccine enters the GC complexed to antibodies and is presented in the light zone on the surfaces of follicular dendritic cells attached to FcγRIIB or CR2 receptors. GC B cells acquire antigen with a probability proportional to their affinity for the antigen. They then receive help from T follicular helper cells with a probability dependent on the relative amount of antigen they acquired. Cells that fail to acquire antigen or receive the latter help die. Cells that succeed can exit the GC to become plasma cells and secrete antibodies, become memory B cells, or migrate to the dark zone, where they proliferate and mutate their antibody genes. The latter cells circulate back to the light zone and become subjected to the same selection process. Antibodies secreted by plasma cells can feedback into the GC and affect the selection process. **(B)** Schematic of the simulations. (Top) Timeline showing dose administration and corresponding antigen levels. (Bottom) GCs are formed following the prime and gradually shrink with time due to decreasing antigen levels. The prime could be low dose (LD) or standard dose (SD). The boost could restore existing GCs (mechanism I) or lead to new GCs seeded by memory B cells formed during the prime (mechanism II). The boost is typically SD.

proliferate and mutate their BCR genes and return to the light zone (39, 43). The latter B cells form the pool for the next generation of the GC reaction. The antibodies produced by plasma cells can feedback into the GC and, by displacing lower affinity antibodies in the immune complexes or by masking antigen, tend to increase the selection stringency (35, 39, 46).

Following dosing, antigen is trafficked to the lymph nodes, where its levels rise rapidly and then decline exponentially (34, 47). Accordingly, we let η rise immediately upon dosing to a pre-determined amount dependent on the vaccine dosage and then decrease with each generation based on the half-life of the administered antigen (**Figure 1B**). With the boost, we considered two scenarios (34, 48, 49): the first where the boost enhanced antigen levels in pre-existing GCs, and the second where it initiated new GCs using memory B cells formed by the prime. We also examined the baseline, control scenario where

the boost initiated GCs *de novo*, independently of the prime. We considered vaccination protocols with low and standard dose prime and a range of prime-boost dosing intervals. We performed multiple stochastic realizations of the simulations for each vaccination protocol and predicted the expected antibody response as an indicator of vaccine efficacy.

Antigen Availability and Its Effect on Selection Stringency

To elucidate affinity maturation in the GC reaction, we first performed simulations with a constant η, set here to 7. (We considered other values of η later.) The GC initially had B cells with low affinity for the target antigen. As the GC reaction proceeded, B cells with increasing affinity were selected in our simulations, marking affinity maturation (**Figure 2A**). Eventually, a stationary distribution of B cells of different affinities was achieved, dominated by B cells with the highest affinities, as observed in previous studies (39) and akin to the mutation-selection balance observed in other evolutionary simulations (50, 51). We focussed on the corresponding evolution of the average affinity of the B cells. As the GC reaction progressed, the average affinity of the B cells increased and reached a plateau (**Figure 2B**). Thus, when η=7, the average affinity of the B cells, determined by the average match-length between the antigen and BCR sequences, plateaued at ~6.7 (**Figure 2B** inset). Note that L=8 in these simulations. We note that match-length is a proxy for affinity. To draw links between match-length and affinities measured using the equilibrium dissociation constant, K_d, we recognize that affinity maturation typically commences with weakly binding antibodies, with K_d~10-100 μM, and can culminate with the strongest binding antibodies, with K_d~1-100 pM (30). In our simulations, these

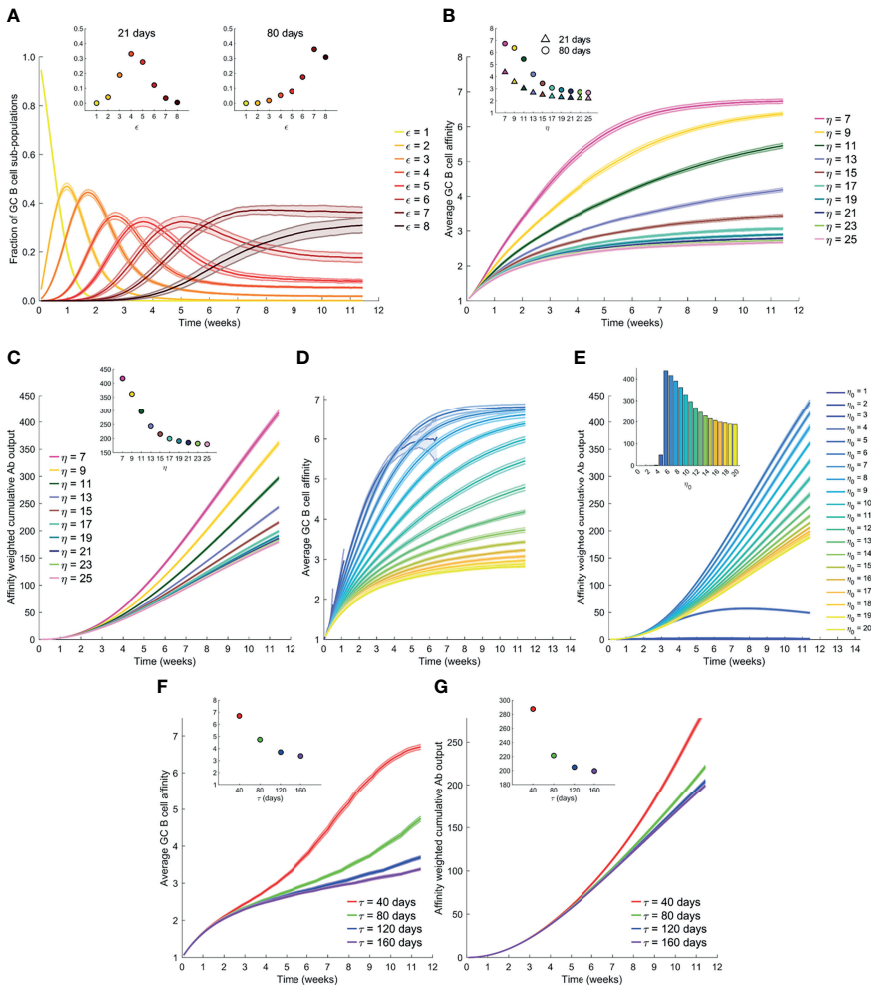

FIGURE 2 | The effect of antigen availability and half-life on the GC reaction. **(A)** Time-evolution of populations of GC B cells of different affinity, ε, for the antigen; η=7. **(B)** Time-evolution of the average affinity of GC B cells for different η. Insets in **(A, B)** The values at day 21 and day 80. **(C)** Time-evolution of the affinity-weighted cumulative antibody output for different η. **(D)** Time-evolution of the average affinity of GC B cells for different initial η, η_0, with antigen half-life, τ=40 d. **(E)** Corresponding cumulative antibody output. **(F)** Time-evolution of the average affinity for different τ, and with η_0 = 20. **(G)** Corresponding cumulative antibody output. Insets in **(C, E, F, G)** Corresponding values at day 80.

extremes span match-lengths 1 to 8, so that a gain of unit match-length would amount approximately to a 10-fold increase in binding affinity (or 10-fold lower K_d).

To examine the effect of antigen availability, we next performed simulations at different values of η. Increasing η resulted in a lower value of the plateau of the average affinity (**Figure 2B**), indicative of weaker selection. Increasing η would correspond to higher vaccine dosages. B cells with lower affinities were selected with higher η because more opportunities were available for antigen acquisition. Thus, the average affinity plateaued at ~3.4 when η=15 and decreased further with larger η (**Figure 2B** inset). This is consistent with the classic observations of poorer affinity maturation with increasing antigen levels (26, 39). In terms of the absolute antibody titres, our simulations predicted that unless the selection stringency was so large that the GC B cell population began to decline causing GC collapse (**Supplementary Figure 1**), the GC B cell population was maintained, leading to a steady output of Abs from the GC (**Supplementary Figure 2**). The lower affinity with increasing η thus resulted in a corresponding decrease in the affinity-weighted cumulative antibody output in our simulations (**Figure 2C**). The latter output was ~417 when η=7 and ~216 when η=15 at 80 d following dosing (**Figure 2C** inset). This affinity-weighted antibody output would serve as a measure of the humoral response elicited by vaccination; it accounts for the effects of both the quality and the quantity of the response. We thus expect it to be proportional to the antibody neutralization titres (or NT_{50} values), determined using neutralization assays and reported experimentally (5, 18, 19). At very high values of η, beyond ~20 in our simulations, the effect of varying η was minimal (**Figures 2B, C**), indicating that at sufficiently high dosages, the effect of varying dosage on the GC reaction may not be significant. At lower η, between 7 and 15 in our simulations, lowering dosage resulted in a substantial gain in the GC response. When η was too low, however, in our simulations, GCs collapsed, as not enough antigen was available for sustaining the B cell population (**Supplementary Figure 1**).

Following vaccination, antigen levels are expected to decline exponentially with time. We therefore next performed simulations with η decreasing with a half-life τ; i.e., $\eta=\eta_0 \exp(-t\times\ln 2/\tau)$, where η_0 is the peak antigen level achieved soon after dosing. Consistently with the above predictions, we found that the average GC B cell affinity decreased with increasing η_0 (**Figure 2D**). However, with low η_0, the GCs were often unsustainable, resulting in early extinguishing of the GCs (see $\eta_0 < 5$ in **Figure 2D**). This resulted in lower GC output, highlighting the quality-quantity trade-off. Increasing η_0 thus yielded lower average affinity but larger numbers of the antibodies produced. The trade-off manifested as a maximum in the affinity-weighted cumulative antibody output at intermediate η_0 (**Figure 2E**). For the parameters chosen, the latter output was minimal for $\eta_0<3$, rose till it attained a peak at $\eta_0 = 6$, and then declined, plateauing as η_0 approached 20. These latter simulations were performed with τ=40 d. How antigen levels quantitatively decay on follicular dendritic cells within GCs relative to that in plasma is not well understood (34, 52, 53). We therefore examined a range of values of τ. We found in our simulations with $\eta_0 = 20$, that the average affinity was higher when τ was lower (**Figure 2F**). Specifically, the average affinity at day 80 from the start of the GC reaction was ~6.7 for τ=40 d and ~3.4 for τ=160 d (**Figure 2F** inset). The faster decay of antigen thus increased the selection stringency within the GC and led to higher affinity B cells. The affinity-weighted cumulative antibody output, accordingly, increased with decreasing τ, consistent with an improved response due to increased selection stringency (**Figure 2G**).

Prime-Boost Vaccination: The Effect of Dosage

We now applied our simulations to mimic the prime-boost vaccination protocols employed in clinical trials (5). Specifically, we considered low dose (which we set using $\eta_0 = 10$) and standard dose ($\eta_0 = 20$) combinations, administered with a dosing interval Δ=28 d mimicking experimental protocols (5, 6, 21). (Our conclusions are not sensitive to these parameter settings; see **Supplementary Figure 3**) An important aspect of the humoral response associated with multiple antigen dosing that remains unknown is whether the subsequent doses modulate GCs formed following the first dose or seed new GCs. GCs have been observed to persist over extended durations following COVID-19 vaccination (24). [Such persistent GCs have been seen following natural infection with other viruses too (25).] If the interval Δ is relatively small, one may expect the boost to modulate ongoing GC reactions, as has been suggested previously (34, 39). However, if Δ is large, then the GCs formed by the prime may collapse due to antigen decay or other mechanisms before the boost, so that the seeding of new GCs by the boost is more likely. In the latter scenario, the effect of the prime must come from the preferential seeding by memory B cells formed following the prime (48, 49, 54). Recruitment of memory B cells into GCs has been suggested, especially those B cells that displayed cross reactivity to other circulating human betacoronaviruses (24). We therefore simulated two limiting scenarios (**Figure 1B**): First, we assumed that the boost modulated existing GCs and seeded no new GCs. Second, we let the boost seed GCs using the memory B cells formed from the prime and not modulate any existing GCs. We also simulated a control case where the boost established new GCs *de novo*, without using memory B cells from the prime, in which case no advantage from the prime is expected.

With the boost modulating existing GCs, our simulations predicted an advantage of the low dose prime over the standard dose prime (blue and red lines in **Figures 3A, B**). The average affinity increased with time more steeply with the low dose until day 28, when the boost was administered (**Figure 3A**). Just prior to boost administration, the average affinity was ~4.9 for the low dose versus ~2.8 for the standard dose prime. Correspondingly, the affinity-weighted cumulative antibody output was higher for the low dose than the standard dose (**Figure 3B**). The diversity of the GC B cell population as well as the affinity of the output B cells reflected these predictions (**Supplementary Figures 4, 5**). The administration of the boost caused an increase

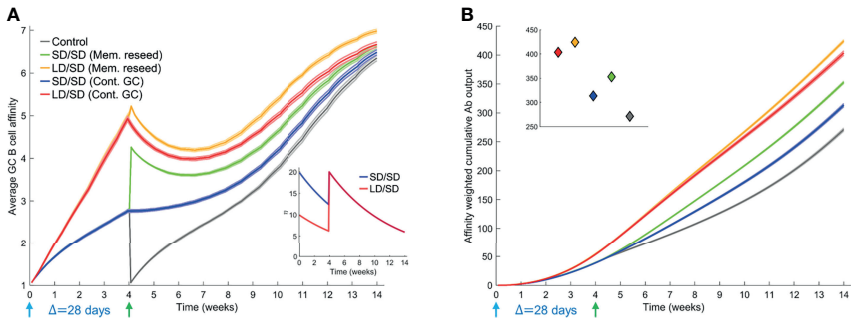

FIGURE 3 | Influence of different prime-boost dosages. **(A)** Time-evolution of the average affinity of GC B cells for different dosing protocols indicated. Inset: The associated antigen levels. **(B)** Time-evolution of the affinity-weighted cumulative antibody output for the cases in **(A)**. Inset: Corresponding values at the final simulation time point. Parameters used: Δ=28 d; τ=40 d; $\eta_{0\ =}$ 10 for LD and $\eta_{0\ =}$ 20 for SD.

in antigen availability (**Figure 3A** inset), relieving the selection stringency. The average affinity thus saw a temporary dip (**Figure 3A**). However, as affinity maturation continued, the higher affinity B cells selected with the low dose prime expanded substantially, yielding a much higher affinity-weighted antibody output than with the standard dose prime (**Figure 3B**). The average affinity and the affinity-weighted cumulative antibody output was higher with the low dose prime than the standard dose prime throughout our simulations.

When we let the boost seed GCs using memory B cells from the prime, the difference between low dose and standard dose prime was smaller in our simulations following the boost (green and orange curves in **Figures 3A, B**). This is because we assumed that only B cells above a certain affinity for the antigen (here, match length ≥ 3; see Methods) could differentiate into memory B cells following stimulation. The advantage of the low dose prime in yielding high affinity B cells was thus reduced. The choice of memory B cells is in keeping with the expectation that low affinity naïve-like B cells may not receive strong enough signals to differentiate into switched memory B cells (55). We recognize that recent studies have suggested that memory B cells may have lower affinity for antigen than plasma cells (56). Thus, we performed simulations where lower affinity B cells differentiated into memory B cells and higher affinity into plasma cells. Our qualitative inferences were unaffected by this alteration (**Supplementary Figure 6**). Even within the memory pool, the low dose prime yielded higher affinity B cells than the standard dose prime, explaining the advantage of the low dose prime in our simulations (**Figure 3A**). The differences in the corresponding affinity-weighted cumulative antibody output (**Figure 3B**) were as expected but commensurately smaller than when the boost seeded existing GCs. Both scenarios yielded better responses than the control case where the boost seeded GCs *de novo* (grey lines in **Figures 3A, B**). We also examined the scenarios where low dose boost was employed following low dose or standard dose prime. The low dose boost did lead to higher GC B cell affinities because of the heightened selection stringency but yielded poorer overall outputs because of the associated increased GC collapse than the standard dose boost in our simulations (**Supplementary Figure 7**). The standard dose boost thus helped consolidate the advantage gained by the low dose prime by relaxing the selection stringency and allowing GC expansion.

Prime-Boost Vaccination: The Effect of Dosing Interval

To assess the influence of the dosing interval, we compared next the antibody responses elicited by two dosing intervals, Δ=28 d and Δ=56 d. We let τ=80 d here to avoid GC collapse following low dose prime with shorter antigen half-lives (**Supplementary Figure 8**). The average GC B cell affinity was significantly higher with Δ=56 d than Δ=28 d when the GCs were allowed to persist until the boost (**Figures 4A, B**). For instance, the average affinity was ~6.6 and ~4.4, respectively, in the two cases, just before the administration of the boost following low dose prime, because affinity maturation continued longer with the longer dosing interval. Besides, the declining antigen levels further increased selection stringency in the latter case. This qualitative trend remained with the standard dose prime. The affinity-weighted cumulative antibody output was also significantly higher with Δ=56 d than Δ=28 d (**Figures 4C, D**). For instance, 28 d after the boost, the output was ~380 and ~174, respectively, in the two cases, when low dose prime was used and the boost modulated existing GCs. With standard dose prime too, the difference was nearly 2-fold. This effect remained whether the boost seeded new GCs or modulated surviving GCs (**Figures 4A–D**), indicating a distinct advantage of the longer interval. The cases all yielded significantly better responses than the control case where the boost elicited GCs *de novo* (**Figures 4A–D**).

Because the selection stringency depended on antigen half-life, τ, we assessed the effect of varying Δ for a range of values of τ. Following recent experiments (9, 12), we also considered much larger values of Δ, ranging from 28 d to 84 d (**Figures 4E, F** and **Supplementary Figure 8**). To evaluate the effect on affinity maturation, we compared the maximum value of the average GC B cell affinity achieved at any time 1 week post the boost (to eliminate transients). We found that at any τ, increasing Δ increased the peak affinity, regardless of the use of low dose or

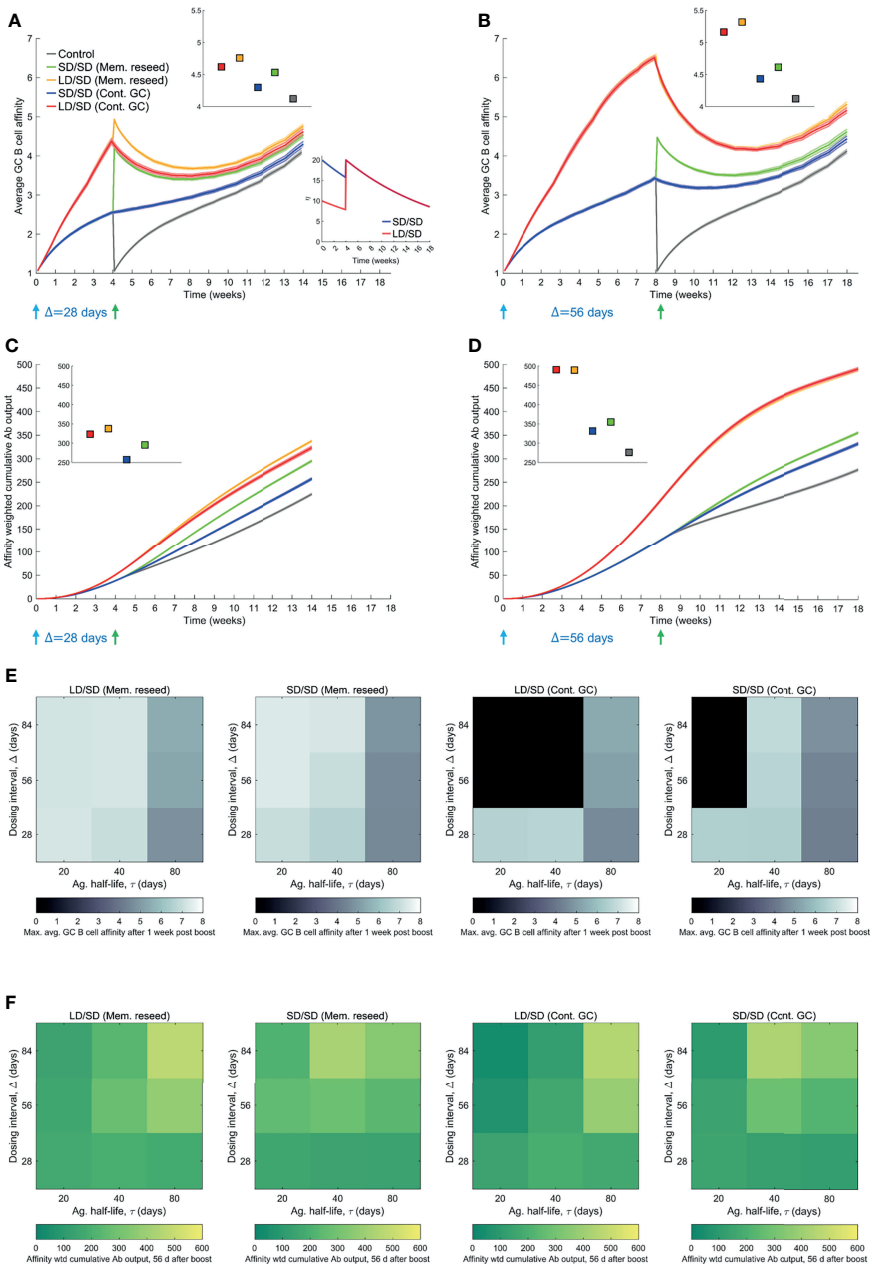

FIGURE 4 | Influence of prime-boost dosing interval. **(A, B)** Average GC B cell affinities, and **(C, D)** affinity-weighted Ab outputs, with prime-boost intervals (Δ) of either 28 d **(A, C)** or 56 d **(B, D)**, and with LD/SD or SD/SD dosing. Bottom inset of **(A)**: LD and SD correspond to η_0 = 10 and 20, respectively, with τ=80 d. Top insets in **(A–D)**: values at the final time point. Heatmaps of **(E)** the maximum GC affinity recorded between 1 week post boost administration and the final time point, and **(F)** the affinity-weighted cumulative Ab output 28 d post the boost, as a function of τ (20, 40 and 80 d) and Δ (4, 8, and 12 weeks) for the two limiting scenarios (Mem. reseed and Cont. GC). Trajectories corresponding to the heatmaps are shown in **Supplementary Figure 8**. Black regions in **(E)** correspond to collapsed GCs. A heatmap of the affinity-weighted cumulative Ab output 56 d post the boost is shown in **Supplementary Figure 8C**.

standard dose prime or whether the boost seeded new GCs or affected existing GCs (**Figure 4E**). Thus, a longer duration yielded a GC response of better quality. Further, the lower was τ, the higher was the peak affinity at any Δ, consistent with stronger selection stringency associated with lower antigen availability (**Figure 4E**).

This latter effect influenced the overall response, combining quality with quantity, which we assessed using the affinity-weighted cumulative antibody output 28 d post the boost (**Figure 4F**). While the overall trend of improved output with longer Δ remained, the trend was more nuanced. The nuances were due to the complex dynamics of the GC responses following

multiple dosing. We examined first the effect of low dose prime. When τ was large, the GC reaction was sustained longer, allowing greater affinity maturation (**Supplementary Figure 8**). Thus, delayed dosing interval would lead to better responses. Indeed, with Δ=56 d and Δ=84 d, our simulations predicted that the cumulative output improved with τ (**Figure 4F**). With Δ=28 d, the GCs may not have expanded sufficiently before the boost. With low τ, leading to high selection stringency, GCs tended to collapse after the boost (**Supplementary Figure 8**). With large τ, the selection stringency was weaker and it therefore took longer for affinities to rise. Consequently, intermediate τ yielded the best response (**Figure 4F**).

With standard dose prime, too, the effects were similar. The GCs were sustained longer as τ increased, but weaker selection due to greater antigen availability led to poorer affinity maturation (**Supplementary Figure 8**). The trade-off tended to yield the best response at intermediate τ. In our simulations, when the boost contributed to existing GCs, it was not efficient in rescuing GCs that were beginning to collapse. Thus, with low and intermediate τ, GCs tended to collapse (**Supplementary Figure 8**). When the boost was assumed to seed new GCs using memory cells from the prime, because the latter had higher affinities for the antigen, the GCs not only survived, but also expanded. The benefit was amplified with delayed dosing as better memory cells became available for seeding the GCs. Thus, as long as τ was not too small, the cumulative output tended to improve with increasing Δ (see τ=40 d and 80 d in **Figure 4F**). (With very small τ, the increased GC collapse compromised the response at high Δ; see τ=20 d in **Figure 4F**). These trends were maintained when the output was considered 56 d post boost (**Supplementary Figure 8**). We note that the trends were not a consequence of the GC collapse brought about by decaying antigen levels. The trends remained even without GC collapse or when the collapse was due to alternative mechanisms such as restricted T_{fh} cell help (57) (**Supplementary Figure 9**). That GCs following COVID-19 vaccination can persist over extended durations (24, 58) suggests that GC shrinkage may be slow *in vivo*. Large dosing intervals would then improve responses, as has been observed in clinical trials (9).

DISCUSSION

Understanding the reasons behind the improved efficacy of COVID-19 vaccines upon delaying the boost dose or using a low dose prime would aid optimal deployment of vaccines, critical to settings with limited supplies. Here, using stochastic simulations of the GC reaction post vaccination, we elucidated plausible mechanistic origins of the improved efficacy. To our knowledge, ours is the first study to employ such simulations to assess the influence of COVID-19 vaccination protocols. The GC reaction is constrained by a quality-quantity trade-off (26, 34, 35, 39, 59): Lower antigen availability in the GC leads to more stringent B cell selection, resulting in the production of higher affinity antibodies but in smaller amounts. Increasing antigen availability reverses these effects. The different dosing protocols used–low versus standard dose prime and different dosing intervals–affect this trade-off. With low dose prime, antigen availability in the GCs is lowered, resulting in the selection of high affinity GC B cells. The boost relaxes the selection stringency and allows the expansion of the selected B cells. Delaying the boost delays the relaxation, resulting in even higher affinity B cells getting selected following the prime. Following the boost, these latter B cells would result in better overall GC responses, explaining the observed improvements in efficacy.

Experimental evidence supports the above reasons. Antibody titres targeting the SARS-CoV-2 spike were measured in individuals administered the boost 8-12 weeks, 15-25 weeks, and 44-45 weeks after the prime (9). The titres were consistently higher in the individuals with the longer dosing intervals. However, interestingly, the titres just before the boost were lower in the individuals with the longer intervals. This was consistent with lower antibody output due to declining antigen availability with time in the GC and the associated GC shrinkage. Furthermore, the higher corresponding selection stringency may have resulted in the selection of GC B cells and memory B cells with higher affinity, which would be expected to rescue shrinking GCs or seed new GCs better, explaining the better responses eventually observed. Improved antibody responses following delayed boost dosing has now been observed with multiple vaccines (9–12).

With dosing intervals smaller than 8-12 weeks or with the low dose prime, the differences in antibody titres have been less apparent (5, 8, 21). Yet, the improvement in vaccine efficacy is substantial (5). While we have argued that this improvement may be due to the improved affinity of the antibodies, direct measurements of affinity are lacking. *In vitro* pseudo-typed virus neutralization efficiency of antibodies isolated 28 d after the boost were not significantly different between individuals administered the low dose prime or the standard dose prime or when both standard doses were administered with a 28 d or 56 d interval (5, 8, 21). It is possible that the improvements in affinity may not be adequate to be manifested as improved *in vitro* neutralization efficiencies, possibly because the stoichiometry of antibody binding to the viral spike proteins that ensures virus neutralization (60–62), which is yet to be estimated for SARS-CoV-2, may be realized in both scenarios. *In vitro* neutralization efficiencies tend to be much higher than corresponding *in vivo* efficiencies (63–65). Nonetheless, greater affinity maturation with lower antigen availability has been long recognized as a hallmark of the GC reaction (26, 34, 35, 39, 45, 59). In independent studies on HIV vaccination, for instance, protocols that allowed antigen levels to rise with time, akin to low dose prime followed by standard dose boost examined here, elicited better antibody responses than protocols that held the antigen levels constant or allowed them to decline with time (34), an effect consistent with the dosing protocols modulating antigen availability and the associated quality-quantity trade-off in the GCs (39).

Previous modeling studies have examined the role of antigen dose and/or prime-boost dosing protocols in the response to vaccination, in the context of other pathogens (34, 36, 39, 45, 66–68). In several studies, low antigen dose has been observed to

increase the affinity of GC B cells produced (36, 39, 45), consistently with experimental observations (26, 59). This observation is also consistent with our present predictions, where lower antigen dose increases selection stringency and leads to faster affinity maturation. That low doses lead to enhanced selection stringency in GCs has been argued by analysis of the heterogeneity of the antibodies produced (59): Soon after antigen exposure, antibodies isolated from sera displayed a range of affinities for the antigen. Interestingly, with time this range shrank and converged to a nearly constant affinity when the antigen dose was low but remained largely intact when the dose was high, indicative of much stronger Darwinian selection with low dose antigen. An important finding from previous studies has also been the need to consolidate the enhanced affinity maturation achieved with low antigen doses by eventually relaxing the selection stringency using higher antigen doses. With low antigen dose, GCs can often collapse due to the lack of antigen required for B cell survival. Thus, with too low an antigen dose, the GCs may collapse before substantial affinity maturation can occur. Consequently, intermediate antigen doses have been argued to yield the best affinity maturation, striking a balance between selection stringency and GC survival (45). It is possible that in some selection scenarios, GC collapse may dominate affinity maturation at low antigen levels. Whether this explains the lack of an improved affinity maturation at low doses predicted in some studies remains to be ascertained (66). In a prime-boost setting, a minimum gap between the doses has been recommended for maximizing the response, to allow for adequate affinity maturation following the prime (67, 69). Others have suggested that exponentially increasing antigen doses in a multi-dose setting may be desirable, as they would not only relax selection stringency with time but also provide adequate antigen for GC expansion, with the possible additional advantage of steering the antibody repertoire towards desired clonotypes (34, 70). These overall findings are consistent with our present predictions of the advantages of low dose prime and delayed boost.

Our simulations predicted a role for antigen half-life in the response to vaccination. With longer half-lives, the response improved upon increasing the dosing interval. With shorter half-lives, if associated GC shrinkage was too drastic before the administration of the boost, the response following the boost was compromised. Shorter dosing intervals then elicited the best response. We note here that the antigen half-life in the GC may be difficult to estimate (34, 52, 53). We therefore examined the effects of a wide range of antigen half-lives. In our simulations, GC shrinkage was typically associated with antigen decay, which we explicitly modeled. In other studies, GC shrinkage has been allowed to occur naturally, due to antigen uptake by GC B cells (45) or limitation of T_{fh} cell help (41, 71). Our results were robust to these alternative modes of GC shrinkage. The advantage of low dose prime in our simulations came from lower antigen levels and hence more stringent selection in the GC. The delayed boost allowed affinity maturation to proceed further. These advantages were amplified by decaying antigen levels, which enhanced selection stringency and expedited affinity maturation. Direct measurements of the evolution of individual GCs post COVID-19 vaccination are not yet available, to our knowledge. That GC B cells and plasmablasts were detectable in high frequencies even 12 weeks after the boost suggests that antigen presented by COVID-19 vaccines may be much longer lasting in the GCs than expected from their half-life in circulation (24, 58). Such prolonged GC responses have been observed in other settings (25). The ranges of antigen decay timescales employed in our simulations were consistent with these latter observations. Future studies may yield accurate estimates of the antigen half-life in GCs, which would not only offer a more direct test of our predictions but also help identify optimal dosing intervals for the different COVID-19 vaccines available.

Quantitative comparison of our predictions with experimental observations is difficult, as has been the case with other modeling studies of the GC reaction (34–36, 39, 40, 42, 46). This is because a number of key biological processes associated with the GC reaction remain to be elucidated, including the link between dosage and the number of GCs seeded, and between measurable antigen levels in circulation and those within individual GCs (22, 23, 34, 35, 39). Only recently have these links begun to be evaluated (37). As a simplification, our simulations have assumed that increased dosage leads to increased antigen availability within GCs while keeping the number of GCs seeded fixed. It is possible that the number of GCs seeded may also increase with dosage but with a commensurately smaller rise in the antigen levels per GC. Future studies that elucidate the links above may help define these quantities better. Nonetheless, the poorer quality of the antibody response with increasing dosage is a widely observed and accepted phenomenon (26, 34, 39), giving us confidence in our findings.

We recognize that other arms of the immune system that could be triggered by the vaccines, particularly T cells, may affect the vaccine efficacies realized (5–9, 13, 14). The strength and timing of the T cell response has been argued to be important in determining the severity of the infection (72), which in turn may affect the estimated vaccine efficacy (73). We have focused here on the antibody response, to which the efficacies have been found to be strongly correlated (18, 19, 73), and which in our simulations offered a qualitative explanation of the effects of the different dosing protocols on vaccine efficacies.

Our simulations have used single, non-mutating antigens as the target of affinity maturation. Such simulations have explained many key features of the GC reaction and the humoral response (39). Simultaneous responses to multiple, evolving antigens are important in settings involving rapidly mutating pathogens, such as HIV, where the diversity of the humoral response may be correlated with viremic control (36, 38, 40, 42, 74). Furthermore, in such settings, it is conceivable that low selection stringency may allow rare precursor B cells, such as those leading to broadly neutralizing antibodies, to get selected (42, 75). With SARS-CoV-2, the spike protein appears reasonably conserved across variants (76), and has allowed the design of vaccines that can generate antibodies with pan-sarbecovirus neutralizing activity (77, 78). Thus, incorporating

diverse antigens and inter-clonal competition are expected not to affect our qualitative inferences regarding SARS-CoV-2 vaccines. Understanding vaccine efficacies quantitatively may require accurate description of antibody diversity given the multiple virus entry pathways accessible to SARS-CoV-2 and the potential synergy associated with blocking the pathways simultaneously (79, 80).

Other hypotheses have been proposed to explain the effects of low dose prime and long dosing intervals, the predominant of which has been the undesirable response to the adenoviral vector in the case of the Oxford/AstraZeneca vaccine that could blunt the response to the boost (81, 82). While these hypotheses remain to be tested, that the effects are now evident with more than one vaccine, including lipid nanoparticle mRNA vaccines that do not use the adenoviral vectors (10–13), suggests that the effects are intrinsic to the responses elicited by the SARS-CoV-2 antigens in the vaccines, supporting our hypothesis. Yet other hypotheses have been proposed in earlier studies on other pathogens, which may have a bearing on COVID-19 vaccines. For instance, low antigen dose, in conjunction with adjuvants, has been argued to improve helper T cell responses (83). Conversely, high dose prime could trigger enhanced helper T cell exhaustion and compromise vaccine responses (84). Vaccination can alter immunodominance patterns of GC B cells (85). Finally, vaccination can influence innate immune responses in complex ways (86). Future studies may examine the contributions of these effects on the influence of low dose prime and/or delayed boost on COVID-19 vaccine efficacies.

In summary, our study offers a plausible explanation of the confounding effects of different dosages and dosing protocols on COVID-19 vaccine efficacies. The resulting insights would inform studies aimed at designing optimal vaccine deployment strategies.

METHODS

Stochastic Simulations of the GC Reaction

We developed the following *in silico* stochastic simulation model of the GC reaction (**Figure 1A**). The model builds on a previous study which examined the role of passive immunization on the GC reaction (39). Here, we adapted it describe the effect of COVID-19 vaccination.

Initialization

We initiated the GC reaction with N=1000 GC B cells of low affinity for the target antigen in the light zone of the GC. This follows observations where low affinity seeder B cells initiate the GC reaction by proliferating rapidly to a steady state size of 1000 cells, following which somatic hypermutation and affinity maturation commence (36, 39). We considered a non-mutating antigen, determined by a randomly chosen string of length L and alphabet of size κ=4. The alphabet size represents the broad classes of amino acids, namely, positively charged, negatively charged, polar, and hydrophobic (42). The B cell receptor (BCR) paratope for each cell is then set by randomly mutating the antigen sequence at L-1 randomly chosen positions. This ensured that the cells in the initial pool all had low affinities for the antigen. The B cells were then allowed to acquire antigen.

Antigen Acquisition

Antigen is presented to B cells as antibody-bound immune complexes on follicular dendritic cell surfaces. The probability with which a B cell successfully acquired the antigen was $f_{Ag} = (\epsilon - \omega + L)/2L$, where ε and ω are the lengths of the longest common substrings of the antigen sequence and those of the associated B cell receptor (BCR) and the presenting antibody, respectively. The latter expression followed from a mechanistic consideration of bond dissociation triggered by the competition between the BCR and the antibody for the antigen (39). Note that antibodies are secreted versions of the BCRs and hence were similarly represented as bit-strings of length L too. The presenting antibodies were produced by plasma cells and re-entered the GC *via* antibody feedback, described below. B cells were selected at random for antigen acquisition, with each B cell selected η times on average. The amount of antigen acquired by a B cell was set equal to the number of successful acquisition attempts, denoted as θ. B cells had to acquire a minimum amount of antigen, denoted θ_c, for them to survive. Surviving cells were eligible to receive help from T follicular helper (T_{fh}) cells. We capped the level of antigen acquired at θ_∞, at which point the B cell may have received saturating levels of stimulatory signals necessary for T_{fh} cell help.

T_{fh} Cell Help

We chose surviving B cells randomly and let each cell receive T_{fh} cell help with the probability $f_T = (\theta - \theta_{min})/(\theta_{max} - \theta_{min})$, where θ_{min} is the minimum antigen acquired by the surviving B cells and θ_{max} (=min(η,θ_∞)) is the maximum antigen acquired. The probability follows from the recognition that T_{fh} cell help depends on the relative and not absolute amount of antigen acquired (23, 39). Cells that did not receive help died. We continued this with every surviving cell and stopped if 250 cells successfully received T_{fh} help.

Cell Fate Decision

Of the cells selected above, we chose 5% randomly to become memory B cells; 5% to become plasma cells; and the rest to migrate to the dark zone of the GC. The memory B cells were constrained to have a minimum affinity for the antigen (55) (here, match length 3) and were allowed to survive long-term. The plasma cells exited the GC, commenced producing antibodies, and died at the rate of 0.015 per generation (**Supplementary Table 1**). To mimic recent experimental observations (56), we also performed simulations where lower affinity B cells differentiated into memory B cells and higher affinity B cells into plasma cells (**Supplementary Figure 6**).

Proliferation And Mutation

The cells in the dark zone were allowed to multiply, with each cell dividing twice. Of the resulting cells, we chose 10% and introduced single random point mutations in their BCR sequences. The latter frequency was chosen following estimates based on the somatic hypermutation frequency suggesting that 1 in 10 GC B cells would be mutated per generation in their antibody variable region genes (23, 36, 39, 42). The two divisions

per cell would bring the cell population back to the N~1000 cells. This completed one generation of B cell evolution in the GC.

Recycling

The resulting cells in the dark zone were all allowed to migrate to the light zone, offering the next generation of cells on which the above process would repeat.

Antibody Feedback

Antibodies produced by plasma cells could traffic back to the GC and influence antigen presentation (35). Accordingly, following estimated trafficking timescales, we let antibodies produced by plasma cells in any generation become the antibodies presenting antigen to B cells two generations later (35, 39). Antibodies were also systemically cleared at the rate of 0.01165 per generation (**Supplementary Table 1**). Ignoring antibody feedback delayed affinity maturation because of lower selection stringency but did not affect our inferences regarding low dose prime and delayed boost (**Supplementary Figure 10**).

Termination

We repeated the above process typically for up to 250 generations (~18 weeks) or until the cell population declined, leading to GC collapse.

Dosing Protocol

We implemented the prime-boost dosing protocol by letting η vary with time as $\eta=\eta_0\exp(-t\times\ln 2/\tau)$, mimicking antigen rise immediately upon dosing (to η_0) and an exponential decline subsequently with half-life τ (34, 39, 47). The decline is assumed to subsume any loss of antigen due to acquisition by B cells. We set η_0 based on whether a low or standard dose was employed. The prime and boost were separated by the duration Δ. Our interest is in large values of Δ and low first dosages, so that at the time of boost administration, the residual antigen is small. Whether memory B cells seed GCs post boost is a topic of active current research (48, 49, 54–56, 87). We therefore considered all potential scenarios, with the boost 1) feeding into existing GCs; 2) seeding new GCs using memory B cells; 3) seeding new GCs using naïve B cells. In scenario 2, we let the memory B cells for seeding the GCs be chosen with a probability proportional to their affinity for the antigen. In other words, the distribution of B cells of different affinities in the seeder pool mimics the distribution of affinity-weighted fractions of memory B cells formed following the prime. We also examined the effect of different fractions (5%-100%) of the seeder B cells being drawn from the memory pool and found no qualitative differences in our predictions (**Supplementary Figure 11**).

Parameter Values

The parameter values employed and their sources are listed in **Supplementary Table 1**.

Quantification of the GC Response

With each parameter setting, we performed 2500 realizations, which we divided into 25 ensembles of 100 GC realizations each (39). The average GC B cell affinity in the g^{th} generation was calculated using,

$$\alpha(g) = \langle \frac{\sum_{i=1}^{100}\sum_{j=1}^{n_i(g)} a_{ij}(g)}{\sum_{i=1}^{100} n_i(g)} \rangle_{25}$$

where a_{ij} was the affinity of the j^{th} B cell among the $n_i(g)$ B cells in the g^{th} generation of the i^{th} realization of an ensemble. The angular brackets represent averaging across the ensembles. The affinity-weighted plasma cell output in the g^{th} generation was

$$w(g) = \langle \sum_{i=1}^{100}\sum_{\epsilon=1}^{L} p_\epsilon^i(g)\frac{\epsilon}{L} \rangle_{25}$$

where $p_\epsilon^i(g)$ was the number of plasma cells with affinity ϵ in the g^{th} generation. If plasma cells died at the per capita rate δ_p, then the affinity-weighted cumulative plasma cell output would be

$$P(g) = \sum_{\varphi=1}^{g} w(\varphi)\exp(-\delta_p(g-\varphi))$$

If the antibody production rate of plasma cells was β per generation (88), the instantaneous affinity-weighted antibody output would be $\beta P(g)$, which given the clearance rate, δ_A, of circulating antibodies yielded the affinity-weighted cumulative antibody output as

$$\gamma(g) = \sum_{\varphi=1}^{g} \beta P(\varphi)\exp(-\delta_A(g-\varphi))$$

We performed the simulations and analysed the results using programs written in MATLAB.

DATA AVAILABILITY STATEMENT

The original contributions presented in the study are included in the article/**Supplementary Material**. Further inquiries can be directed to the corresponding author.

AUTHOR CONTRIBUTIONS

AG, RD, and ND designed research. AG and RD performed research. AG, SM, PP, RD, and ND contributed new reagents and analytic tools and analysed data. ND wrote the paper. All authors contributed to the article and approved the submitted version.

SUPPLEMENTARY MATERIAL

The Supplementary Material for this article can be found online at: https://www.frontiersin.org/articles/10.3389/fimmu.2021.776933/full#supplementary-material

REFERENCES

1. Wouters OJ, Shadlen KC, Salcher-Konrad M, Pollard AJ, Larson HJ, Teerawattananon Y, et al. Challenges in Ensuring Global Access to COVID-19 Vaccines: Production, Affordability, Allocation, and Deployment. *Lancet* (2021) 397:1023–34. doi: 10.1016/S0140-6736(21)00306-8
2. Forni G, Mantovani A. COVID-19 Vaccines: Where We Stand and Challenges Ahead. *Cell Death Differ* (2021) 28:626–39. doi: 10.1038/s41418-020-00720-9
3. Saad-Roy CM, Morris SE, Metcalf CJE, Mina MJ, Baker RE, Farrar J, et al. Epidemiological and Evolutionary Considerations of SARS-CoV-2 Vaccine Dosing Regimes. *Science* (2021) 372:363–70. doi: 10.1126/science.abg8663
4. Bubar KM, Reinholt K, Kissler SM, Lipsitch M, Cobey S, Grad YH, et al. Model-Informed COVID-19 Vaccine Prioritization Strategies by Age and Serostatus. *Science* (2021) 371:916–21. doi: 10.1126/science.abe6959
5. Voysey M, Costa Clemens SA, Madhi SA, Weckx LY, Folegatti PM, Aley PK, et al. Single-Dose Administration and the Influence of the Timing of the Booster Dose on Immunogenicity and Efficacy of ChAdOx1 Ncov-19 (AZD1222) Vaccine: A Pooled Analysis of Four Randomised Trials. *Lancet* (2021) 397:881–91. doi: 10.1016/s0140-6736(21)00432-3
6. Voysey M, Clemens SAC, Madhi SA, Weckx LY, Folegatti PM, Aley PK, et al. Safety and Efficacy of the ChAdOx1 Ncov-19 Vaccine (AZD1222) Against SARS-CoV-2: An Interim Analysis of Four Randomised Controlled Trials in Brazil, South Africa, and the UK. *Lancet* (2021) 397:99–111. doi: 10.1016/S0140-6736(20)32661-1
7. Folegatti PM, Ewer KJ, Aley PK, Angus B, Becker S, Belij-Rammerstorfer S, et al. Safety and Immunogenicity of the ChAdOx1 Ncov-19 Vaccine Against SARS-CoV-2: A Preliminary Report of a Phase 1/2, Single-Blind, Randomised Controlled Trial. *Lancet* (2020) 396:467–78. doi: 10.1016/S0140-6736(20)31604-4
8. Ramasamy MN, Minassian AM, Ewer KJ, Flaxman AL, Folegatti PM, Owens DR, et al. Safety and Immunogenicity of ChAdOx1 Ncov-19 Vaccine Administered in a Prime-Boost Regimen in Young and Old Adults (COV002): A Single-Blind, Randomised, Controlled, Phase 2/3 Trial. *Lancet* (2021) 396:1979–93. doi: 10.1016/S0140-6736(20)32466-1
9. Flaxman A, Marchevsky N, Jenkin D, Aboagye J, Aley PK, Angus BJ, et al. Reactogenicity and Immunogenicity After a Late Second Dose or a Third Dose of ChAdOx1 nCoV-19 in the UK: A substudy of two randomised controlled trials (COV001 and COV002). *Lancet* (2021) 398:981–90. doi: 10.1016/S0140-6736(21)01699-8
10. Parry H, Bruton R, Stephens C, Brown K, Amirthalingam G, Hallis B, et al. Extended Interval BNT162b2 Vaccination Enhances Peak Antibody Generation in Older People. *medRxiv* (2021). doi: 10.1101/2021.05.15.21257017
11. Victoria H, Victor F, Matthew I, Terrance K, Beata M-K, Vathany K, et al. Delayed Interval BNT162b2 mRNA COVID-19 Vaccination Provides Robust Immunity. *Nat Portfolio* (2021). doi: 10.21203/rs.3.rs-793234/v1
12. Payne R, Longet S, Austin J, Skelly D, Dejnirattisai W, Adele S, et al. *Sustained T Cell Immunity, Protection and Boosting Using Extended Dosing Intervals of BNT162b2 mRNA Vaccine* (2021). Available at: https://www.pitch-study.org/PITCH_Dosing_Interval_23072021.pdf.
13. Mateus J, Dan JM, Zhang Z, Moderbacher CR, Lammers M, Goodwin B, et al. Low Dose mRNA-1273 COVID-19 Vaccine Generates Durable Memory Enhanced by Crossreactive T Cells. *Science* (2021) 374. doi: 10.1126/science.abj9853
14. Sadarangani M, Marchant A, Kollmann TR. Immunological Mechanisms of Vaccine-Induced Protection Against COVID-19 in Humans. *Nat Rev Immunol* (2021) 21:475–84. doi: 10.1038/s41577-021-00578-z
15. Baden LR, El Sahly HM, Essink B, Kotloff K, Frey S, Novak R, et al. Efficacy and Safety of the mRNA-1273 SARS-CoV-2 Vaccine. *N Engl J Med* (2021) 384:403–16. doi: 10.1056/NEJMoa2035389
16. Logunov DY, Dolzhikova IV, Shcheblyakov DV, Tukhvatulin AI, Zubkova OV, Dzharullaeva AS, et al. Safety and Efficacy of an Rad26 and Rad5 Vector-Based Heterologous Prime-Boost COVID-19 Vaccine: An Interim Analysis of a Randomised Controlled Phase 3 Trial in Russia. *Lancet* (2021) 397:671–81. doi: 10.1016/S0140-6736(21)00234-8
17. Polack FP, Thomas SJ, Kitchin N, Absalon J, Gurtman A, Lockhart S, et al. Safety and Efficacy of the BNT162b2 mRNA COVID-19 Vaccine. *N Engl J Med* (2020) 383:2603–15. doi: 10.1056/NEJMoa2034577
18. Khoury DS, Cromer D, Reynaldi A, Schlub TE, Wheatley AK, Juno JA, et al. Neutralizing Antibody Levels Are Highly Predictive of Immune Protection From Symptomatic SARS-CoV-2 Infection. *Nat Med* (2021) 27:1205–11. doi: 10.1038/s41591-021-01377-8
19. Earle KA, Ambrosino DM, Fiore-Gartland A, Goldblatt D, Gilbert PB, Siber GR, et al. Evidence for Antibody as a Protective Correlate for COVID-19 Vaccines. *Vaccine* (2021) 39:4423–8. doi: 10.1016/j.vaccine.2021.05.063
20. Krammer F. A Correlate of Protection for SARS-CoV-2 Vaccines Is Urgently Needed. *Nat Med* (2021) 27:1147–8. doi: 10.1038/s41591-021-01432-4
21. Barrett JR, Belij-Rammerstorfer S, Dold C, Ewer KJ, Folegatti PM, Gilbride C, et al. Phase 1/2 Trial of SARS-CoV-2 Vaccine ChAdOx1 Ncov-19 With a Booster Dose Induces Multifunctional Antibody Responses. *Nat Med* (2021) 27:279–88. doi: 10.1038/s41591-020-01179-4
22. Cyster JG, Allen CDC. B Cell Responses: Cell Interaction Dynamics and Decisions. *Cell* (2019) 177:524–40. doi: 10.1016/j.cell.2019.03.016
23. Victora GD, Nussenzweig MC. Germinal Centers. *Annu Rev Immunol* (2012) 30:429–57. doi: 10.1146/annurev-immunol-020711-075032
24. Turner JS, O'Halloran JA, Kalaidina E, Kim W, Schmitz AJ, Zhou JQ, et al. SARS-CoV-2 mRNA Vaccines Induce Persistent Human Germinal Centre Responses. *Nature* (2021) 596:109–13. doi: 10.1038/s41586-021-03738-2
25. Davis CW, Jackson KJL, McElroy AK, Halfmann P, Huang J, Chennareddy C, et al. Longitudinal Analysis of the Human B Cell Response to Ebola Virus Infection. *Cell* (2019) 177:1566–82.e17. doi: 10.1016/j.cell.2019.04.036
26. Eisen HN, Siskind GW. Variations in Affinities of Antibodies During the Immune Response. *Biochemistry* (1964) 3:996–1008. doi: 10.1021/bi00895a027
27. Bonsignori M, Zhou T, Sheng Z, Chen L, Gao F, Joyce MG, et al. Maturation Pathway From Germline to Broad HIV-1 Neutralizer of a CD4-Mimic Antibody. *Cell* (2016) 165:449–63. doi: 10.1016/j.cell.2016.02.022
28. Foote J, Eisen HN. Kinetic and Affinity Limits on Antibodies Produced During Immune Responses. *Proc Natl Acad Sci USA* (1995) 92:1254–6. doi: 10.1073/pnas.92.5.1254
29. Foote J, Eisen HN. Breaking the Affinity Ceiling for Antibodies and T Cell Receptors. *Proc Natl Acad Sci USA* (2000) 97:10679–81. doi: 10.1073/pnas.97.20.10679
30. Desikan R, Antia R, Dixit NM. Physical 'Strength' of the Multi-Protein Chain Connecting Immune Cells: Does the Weakest Link Limit Antibody Affinity Maturation? *Bioessays* (2021) 43:e2000159. doi: 10.1002/bies.202000159
31. Tas JM, Mesin L, Pasqual G, Targ S, Jacobsen JT, Mano YM, et al. Visualizing Antibody Affinity Maturation in Germinal Centers. *Science* (2016) 351:1048–54. doi: 10.1126/science.aad3439
32. Natkanski E, Lee WY, Mistry B, Casal A, Molloy JE, Tolar P. B Cells Use Mechanical Energy to Discriminate Antigen Affinities. *Science* (2013) 340:1587–90. doi: 10.1126/science.1237572
33. Kwak K, Quizon N, Sohn H, Saniee A, Manzella-Lapeira J, Holla P, et al. Intrinsic Properties of Human Germinal Center B Cells Set Antigen Affinity Thresholds. *Sci Immunol* (2018) 3:eaau6598. doi: 10.1126/sciimmunol.aau6598
34. Tam HH, Melo MB, Kang M, Pelet JM, Ruda VM, Foley MH, et al. Sustained Antigen Availability During Germinal Center Initiation Enhances Antibody Responses to Vaccination. *Proc Natl Acad Sci USA* (2016) 113:E6639–48. doi: 10.1073/pnas.1606050113
35. Zhang Y, Meyer-Hermann M, George LA, Figge MT, Khan M, Goodall M, et al. Germinal Center B Cells Govern Their Own Fate *via* Antibody Feedback. *J Exp Med* (2013) 210:457–64. doi: 10.1084/jem.20120150
36. Wang S, Mata-Fink J, Kriegsman B, Hanson M, Irvine DJ, Eisen HN, et al. Manipulating the Selection Forces During Affinity Maturation to Generate Cross-Reactive HIV Antibodies. *Cell* (2015) 160:785–97. doi: 10.1016/j.cell.2015.01.027
37. Kato Y, Abbott RK, Freeman BL, Haupt S, Groschel B, Silva M, et al. Multifaceted Effects of Antigen Valency on B Cell Response Composition and Differentiation *In Vivo*. *Immunity* (2020) 53:548–63.e8. doi: 10.1016/j.immuni.2020.08.001
38. Schoofs T, Klein F, Braunschweig M, Kreider EF, Feldmann A, Nogueira L, et al. HIV-1 Therapy With Monoclonal Antibody 3BNC117 Elicits Host Immune Responses Against HIV-1. *Science* (2016) 352:997–1001. doi: 10.1126/science.aaf0972
39. Garg AK, Desikan R, Dixit NM. Preferential Presentation of High-Affinity Immune Complexes in Germinal Centers can Explain How Passive Immunization Improves the Humoral Response. *Cell Rep* (2019) 29:3946–57.e5. doi: 10.1016/j.celrep.2019.11.030

40. De Boer RJ, Perelson AS. How Germinal Centers Evolve Broadly Neutralizing Antibodies: The Breadth of the Follicular Helper T Cell Response. *J Virol* (2017) 91:e00983–17. doi: 10.1128/JVI.00983-17
41. Meyer-Hermann M, Mohr E, Pelletier N, Zhang Y, Victora Gabriel D. Toellner K-M. A Theory of Germinal Center B Cell Selection, Division, and Exit. *Cell Rep* (2012) 2:162–74. doi: 10.1016/j.celrep.2012.05.010
42. Luo S, Perelson AS. Competitive Exclusion by Autologous Antibodies can Prevent Broad HIV-1 Antibodies From Arising. *Proc Natl Acad Sci USA* (2015) 112:11654–9. doi: 10.1073/pnas.1505207112
43. Oprea M, Perelson AS. Somatic Mutation Leads to Efficient Affinity Maturation When Centrocytes Recycle Back to Centroblasts. *J Immunol* (1997) 158:5155–62.
44. Kepler TB, Perelson AS. Cyclic Re-Entry of Germinal Center B Cells and the Efficiency of Affinity Maturation. *Immunol Today* (1993) 14:412–5. doi: 10.1016/0167-5699(93)90145-B
45. Molari M, Eyer K, Baudry J, Cocco S, Monasson R. Quantitative Modeling of the Effect of Antigen Dosage on B-Cell Affinity Distributions in Maturating Germinal Centers. *eLife* (2020) 9:e55678. doi: 10.7554/eLife.55678
46. Zarnitsyna VI, Lavine J, Ellebedy A, Ahmed R, Antia R. Multi-Epitope Models Explain How Pre-Existing Antibodies Affect the Generation of Broadly Protective Responses to Influenza. *PloS Pathog* (2016) 12:e1005692. doi: 10.1371/journal.ppat.1005692
47. Pape KA, Catron DM, Itano AA, Jenkins MK. The Humoral Immune Response Is Initiated in Lymph Nodes by B Cells That Acquire Soluble Antigen Directly in the Follicles. *Immunity* (2007) 26:491–502. doi: 10.1016/j.immuni.2007.02.011
48. Pape KA, Jenkins MK. Do Memory B Cells Form Secondary Germinal Centers?: It Depends. *Cold Spring Harb Perspect Biol* (2018) 10:a029116. doi: 10.1101/cshperspect.a029116
49. Shlomchik MJ. Do Memory B Cells Form Secondary Germinal Centers?: Yes and No. *Cold Spring Harb Perspect Biol* (2018) 10:a029405. doi: 10.1101/cshperspect.a029405
50. Tripathi K, Balagam R, Vishnoi NK, Dixit NM. Stochastic Simulations Suggest That HIV-1 Survives Close to Its Error Threshold. *PloS Comput Biol* (2012) 8: e1002684. doi: 10.1371/journal.pcbi.1002684
51. Gadhamsetty S, Dixit NM. Estimating Frequencies of Minority Nevirapine-Resistant Strains in Chronically HIV-1-Infected Individuals Naive to Nevirapine by Using Stochastic Simulations and a Mathematical Model. *J Virol* (2010) 84:10230–40. doi: 10.1128/JVI.01010-10
52. Heesters BA, van der Poel CE, Das A, Carroll MC. Antigen Presentation to B Cells. *Trends Immunol* (2016) 37:844–54. doi: 10.1016/j.it.2016.10.003
53. Heesters BA, Myers RC, Carroll MC. Follicular Dendritic Cells: Dynamic Antigen Libraries. *Nat Rev Immunol* (2014) 14:495–504. doi: 10.1038/nri3689
54. McHeyzer-Williams LJ, Dufaud C, McHeyzer-Williams MG. Do Memory B Cells Form Secondary Germinal Centers?: Impact of Antibody Class and Quality of Memory T-Cell Help at Recall. *Cold Spring Harb Perspect Biol* (2018) 10:a028878. doi: 10.1101/cshperspect.a028878
55. Weisel F, Shlomchik M. Memory B Cells of Mice and Humans. *Ann Rev Immunol* (2017) 35:255–84. doi: 10.1146/annurev-immunol-041015-055531
56. Viant C, Weymar GHJ, Escolano A, Chen S, Hartweger H, Cipolla M, et al. Antibody Affinity Shapes the Choice Between Memory and Germinal Center B Cell Fates. *Cell* (2020) 183:1298–311.e11. doi: 10.1016/j.cell.2020.09.063
57. Jacobsen JT, Hu W, Castro TBR, Solem S, Galante A, Lin Z, et al. Expression of Foxp3 by T Follicular Helper Cells in End-Stage Germinal Centers. *Science* (2021) 373:eabe5146. doi: 10.1126/science.abe5146
58. Kim W, Zhou JQ, Sturtz AJ, Horvath SC, Schmitz AJ, Lei T, et al. Germinal Centre-Driven Maturation of B Cell Response to SARS-CoV-2 Vaccination. *bioRxiv* (2021). doi: 10.1101/2021.10.31.466651
59. Kang M, Eisen TJ, Eisen EA, Chakraborty AK, Eisen HN. Affinity Inequality Among Serum Antibodies That Originate in Lymphoid Germinal Centers. *PloS One* (2015) 10:e0139222. doi: 10.1371/journal.pone.0139222
60. Brandenberg OF, Magnus C, Rusert P, Gunthard HF, Regoes RR, Trkola A. Predicting HIV-1 Transmission and Antibody Neutralization Efficacy *In Vivo* From Stoichiometric Parameters. *PloS Pathog* (2017) 13:e1006313. doi: 10.1371/journal.ppat.1006313
61. Mulampaka SN, Dixit NM. Estimating the Threshold Surface Density of Gp120-CCR5 Complexes Necessary for HIV-1 Envelope-Mediated Cell-Cell Fusion. *PloS One* (2011) 6:e19941. doi: 10.1371/journal.pone.0019941
62. Padmanabhan P, Dixit NM. Mathematical Model of Viral Kinetics *In Vitro* Estimates the Number of E2-CD81 Complexes Necessary for Hepatitis C Virus Entry. *PloS Comput Biol* (2011) 7:e1002307. doi: 10.1371/journal.pcbi.1002307
63. van Gils MJ, Sanders RW. *In Vivo* Protection by Broadly Neutralizing HIV Antibodies. *Trends Microbiol* (2014) 22:550–1. doi: 10.1016/j.tim.2014.08.006
64. Chigutsa E, O'Brien L, Ferguson-Sells L, Long A, Chien J. Population Pharmacokinetics and Pharmacodynamics of the Neutralizing Antibodies Bamlanivimab and Etesevimab in Patients With Mild to Moderate COVID-19 Infection. *Clin Pharm Ther* (2021) 110:1302–10. doi: 10.1002/cpt.2420
65. Maisonnasse P, Aldon Y, Marc A, Marlin R, Dereuddre-Bosquet N, Kuzmina NA, et al. COVA1-18 Neutralizing Antibody Protects Against SARS-CoV-2 in Three Preclinical Models. *Nat Commun* (2021) 12:6097. doi: 10.1038/s41467-021-26354-0
66. Meyer-Hermann ME, Maini PK, Iber D. An Analysis of B Cell Selection Mechanisms in Germinal Centers. *Math Med Biol* (2006) 23:255–77. doi: 10.1093/imammb/dql012
67. Castiglione F, Mantile F, De Berardinis P, Prisco A. How the Interval Between Prime and Boost Injection Affects the Immune Response in a Computational Model of the Immune System. *Comput Math Methods Med* (2012) 2012:842329. doi: 10.1155/2012/842329
68. Rhodes SJ, Knight GM, Kirschner DE, White RG, Evans TG. Dose Finding for New Vaccines: The Role for Immunostimulation/Immunodynamic Modelling. *J Theoret Biol* (2019) 465:51–5. doi: 10.1016/j.jtbi.2019.01.017
69. Giorgi M, Desikan R, van der Graaf PH, Kierzek AM. Application of Quantitative Systems Pharmacology to Guide the Optimal Dosing of COVID-19 Vaccines. *CPT Pharmacometrics Syst Pharmacol* (2021) 10:1130–3. doi: 10.1002/psp4.12700
70. Cirelli KM, Carnathan DG, Nogal B, Martin JT, Rodriguez OL, Upadhyay AA, et al. Slow Delivery Immunization Enhances HIV Neutralizing Antibody and Germinal Center Responses *via* Modulation of Immunodominance. *Cell* (2019) 177:1153–71.e28. doi: 10.1016/j.cell.2019.04.012
71. Pélissier A, Akrout Y, Jahn K, Kuipers J, Klein U, Beerenwinkel N, et al. Computational Model Reveals a Stochastic Mechanism Behind Germinal Center Clonal Bursts. *Cells* (2020) 9:1448. doi: 10.3390/cells9061448
72. Chatterjee B, Sandhu HS, Dixit NM. The Relative Strength and Timing of Innate Immune and CD8 T-Cell Responses Underlie the Heterogeneous Outcomes of SARS-CoV-2 Infection. *medRxiv* (2021). doi: 10.1101/2021.06.15.21258935
73. Padmanabhan P, Desikan R, Dixit NM. Modelling the Population-Level Protection Conferred by COVID-19 Vaccination. *medRxiv* (2021). doi: 10.1101/2021.03.16.21253742
74. Wang S. Optimal Sequential Immunization can Focus Antibody Responses Against Diversity Loss and Distraction. *PloS Comput Biol* (2017) 13:e1005336. doi: 10.1371/journal.pcbi.1005336
75. Abbott RK, Lee JH, Menis S, Skog P, Rossi M, Ota T, et al. Precursor Frequency and Affinity Determine B Cell Competitive Fitness in Germinal Centers, Tested With Germline-Targeting HIV Vaccine Immunogens. *Immunity* (2018) 48:133–46.e6. doi: 10.1016/j.immuni.2017.11.023
76. Harvey WT, Carabelli AM, Jackson B, Gupta RK, Thomson EC, Harrison EM, et al. SARS-CoV-2 Variants, Spike Mutations and Immune Escape. *Nat Rev Microbiol* (2021) 19:409–24. doi: 10.1038/s41579-021-00573-0
77. Starr TN, Czudnochowski N, Liu Z, Zatta F, Park Y-J, Addetia A, et al. SARS-CoV-2 RBD Antibodies That Maximize Breadth and Resistance to Escape. *Nature* (2021) 597:97–102. doi: 10.1038/s41586-021-03807-6
78. Tan C-W, Chia W-N, Young BE, Zhu F, Lim B-L, Sia W-R, et al. Pan-Sarbecovirus Neutralizing Antibodies in BNT162b2-Immunized SARS-CoV-1 Survivors. *New Engl J Med* (2021) 385:1401–6. doi: 10.1056/NEJMoa2108453
79. Padmanabhan P, Desikan R, Dixit NM. Targeting TMPRSS2 and Cathepsin B/L Together may be Synergistic Against SARS-CoV-2 Infection. *PloS Comput Biol* (2020) 16:e1008461. doi: 10.1371/journal.pcbi.1008461
80. Kreutzberger AJB, Sanyal A, Ojha R, Pyle JD, Vapalahti O, Balistreri G, et al. Synergistic Block of SARS-CoV-2 Infection by Combined Drug Inhibition of the Host Entry Factors PIKfyve Kinase and TMPRSS2 Protease. *J Virol* (2021) 95:e00975–21. doi: 10.1128/JVI.00975-21
81. Callaway E. Why Oxford's Positive COVID Vaccine Results Are Puzzling Scientists. *Nature* (2020) 588:16–8. doi: 10.1038/d41586-020-03326-w
82. Zamai L, Rocchi MBL. Hypothesis: Possible Influence of Antivector Immunity and SARS-CoV-2 Variants on Efficacy of ChAdOx1 Ncov-19 Vaccine. *Br J Pharm* (2021). doi: 10.1111/bph.15620

83. Billeskov R, Wang Y, Solaymani-Mohammadi S, Frey B, Kulkarni S, Andersen P, et al. Low Antigen Dose in Adjuvant-Based Vaccination Selectively Induces CD4 T Cells With Enhanced Functional Avidity and Protective Efficacy. *J Immunol* (2017) 198:3494. doi: 10.4049/jimmunol.1600965
84. Billeskov R, Lindenstrøm T, Woodworth J, Vilaplana C, Cardona P-J, Cassidy JP, et al. High Antigen Dose Is Detrimental to Post-Exposure Vaccine Protection Against Tuberculosis. *Front Immunol* (2018) 8:1973. doi: 10.3389/fimmu.2017.01973
85. Amitai A, Sangesland M, Barnes RM, Rohrer D, Lonberg N, Lingwood D, et al. Defining and Manipulating B Cell Immunodominance Hierarchies to Elicit Broadly Neutralizing Antibody Responses Against Influenza Virus. *Cell Syst* (2020) 11:573–88.e9. doi: 10.1016/j.cels.2020.09.005
86. Palgen J-L, Feraoun Y, Dzangué-Tchoupou G, Joly C, Martinon F, Le Grand R, et al. Optimize Prime/Boost Vaccine Strategies: Trained Immunity as a New Player in the Game. *Front Immunol* (2021) 12:612747. doi: 10.3389/fimmu.2021.612747
87. Mesin L, Schiepers A, Ersching J, Barbulescu A, Cavazzoni CB, Angelini A, et al. Restricted Clonality and Limited Germinal Center Reentry Characterize Memory B Cell Reactivation by Boosting. *Cell* (2020) 180:92–106.e11. doi: 10.1016/j.cell.2019.11.032
88. Roberts K, Alberts B, Johnson A, Walter P, Hunt T. *Molecular Biology of the Cell. 4th edition*. New York: Garland Science (2002).

Conflict of Interest: The authors declare that the research was conducted in the absence of any commercial or financial relationships that could be construed as a potential conflict of interest.

Publisher's Note: All claims expressed in this article are solely those of the authors and do not necessarily represent those of their affiliated organizations, or those of the publisher, the editors and the reviewers. Any product that may be evaluated in this article, or claim that may be made by its manufacturer, is not guaranteed or endorsed by the publisher.